Morphological Effects of Ballistic Impact on Fabrics of Highly Drawn Polyethylene Fibers

C. RICHARD DESPER,[1,*] SAMUEL H. COHEN,[2] AND ABRAM O. KING[2]

[1]U.S. Army Materials Technology Laboratory, Watertown, Massachusetts 02172, and [2]U.S. Army Natick Research Development & Engineering Center, Natick, Massachusetts 01065

SYNOPSIS

Changes in crystalline structure of high-tenacity ultra-high-molecular-weight polyethylene fabric brought on by ballistic impact from a small projectile were determined by X-ray diffractometry. A suitable X-ray diffraction method that averages out the fiber orientation effects in the diffraction pattern was used. The Spectra 1000™ polyethylene fabrics were successfully characterized in terms of both the predominant orthorhombic and the minor monoclinic crystal content. Crystallinity values for the undamaged fabric are consistent from sample to sample and show an average orthorhombic fraction of 0.61 and an average monoclinic fraction of 0.04. Fabric damage by the projectile impact results in either an increase in monoclinic fraction, attributed to recrystallization at temperatures nearing the normal polyethylene melting point, or disappearance of monoclinic material as that temperature is exceeded. The latter predominates where ballistic penetration is complete. However, actual melting need not be involved: Transformation to the hexagonal ("rotator") phase and the disappearance of the monoclinic phase could have occurred rather than true melting.

INTRODUCTION

X-ray diffraction analysis has been conducted on test panels of candidate personnel armor materials made from Spectra 1000™ polyethylene fibers of ultrahigh orientation. The focus of these experiments has been on the determination of crystallinity content for both the predominating orthorhombic crystal form and the metastable monoclinic crystal form. A total of 16 ballistically tested impact sites has been examined in the test panels, and crystalline content was determined twice for each site—once near the point of ballistic impact and a second time at an undamaged area distant from the impact point.

The diffraction peaks observed were: the monoclinic (001) reflection and the orthorhombic (110) and (200) reflections; a broad amorphous halo was also observed. The predominating crystalline form for all fabric samples is the orthorhombic form, characterized by the peaks at 21.5 and 23.8°, using copper $K\alpha$ radiation with a wavelength of 1.5418 Å. In some instances, the monoclinic phase, characterized by a peak at 19.4°, is also observed.

Bunn[1] was the first to determine the orthorhombic crystalline form of polyethylene. Since then, quantitative studies of polyethylene crystallinity, crystallite size, and crystalline disorder have been carried out by (among others) Kavesh and Schultz,[2] using unoriented specimens, and by Busing,[3] on the same Spectra 1000™ grade of polyethylene fiber used in the fabrics examined here.

The monoclinic phase of polyethylene usually appears under special processing conditions, such as cold working below the usual polyethylene melting point, and has been observed by Slichter,[4] Tanaka et al.,[5] Seto et al.,[6] Magill et al.,[7] Fatou et al.,[8] and Mead et al.[9] In general, higher molecular weights also favor the formation of the monoclinic phase, perhaps through its effect on the polymer mechanical relaxation spectrum.

* To whom correspondence should be addressed.

Journal of Applied Polymer Science, Vol. 47, 1129–1142 (1993)

Published by John Wiley & Sons, Inc. CCC 0021-8995/93/071129-14

EXPERIMENTAL

The X-ray diffraction instrument used comprises a Picker four-circle diffractometer, a PDP-11/23 computer for control of the four diffractometer angles, a Technology for Energy Corporation position-sensitive proportional counter, and a Lecroy 3500 multiple-channel analyzer to record the counter output. The fabric samples are mounted in the instrument, as shown in Figure 1, in the symmetrical transmission position. The instrument can rotate the specimen using its χ motion, while a second motion controls 2θ, the angle between the incident beam $\mathbf{S}_0$ and the diffracted beam $\mathbf{S}_1$. The diffraction vector $\mathbf{S}$, which is the difference $\mathbf{S}_1 - \mathbf{S}_0$ between $\mathbf{S}_1$ and $\mathbf{S}_0$, always lies in the fabric plane, defined by the two sets of fibers F_1 and F_2. The data acquisition method averaged out the anisotropic diffraction pattern using a suitable weighting procedure to yield the pattern of a hypothetical equivalent random orientation sample, modified for the requirements of a fabric sample consisting of two populations of fibers at right angles to each other. This method is described in the Appendix.

The X-ray beam has a circular cross-section of 0.5 mm diameter and, at a monochromatic wavelength of 1.542 Å, is capable of penetrating the thickness of the test panel without serious absorption effects. Thus, the effective sample is a cylindrical section of fabric of 0.5 mm diameter and height equal to the fabric thickness. The beam diameter is considerably larger than the fiber yarn diameter but a factor of 10 smaller than the 0.22-in (5.6 mm) caliber projectile size. (The projectiles were blunt cylinders.) Damaged zone patterns were taken by placing the beam on fabric material as close as possible to the point of ballistic impact. In all undamaged zone (control) patterns, the target area of the X-ray beam was placed 1 in (25 mm) from the damage zone and not along a fiber axis line with the

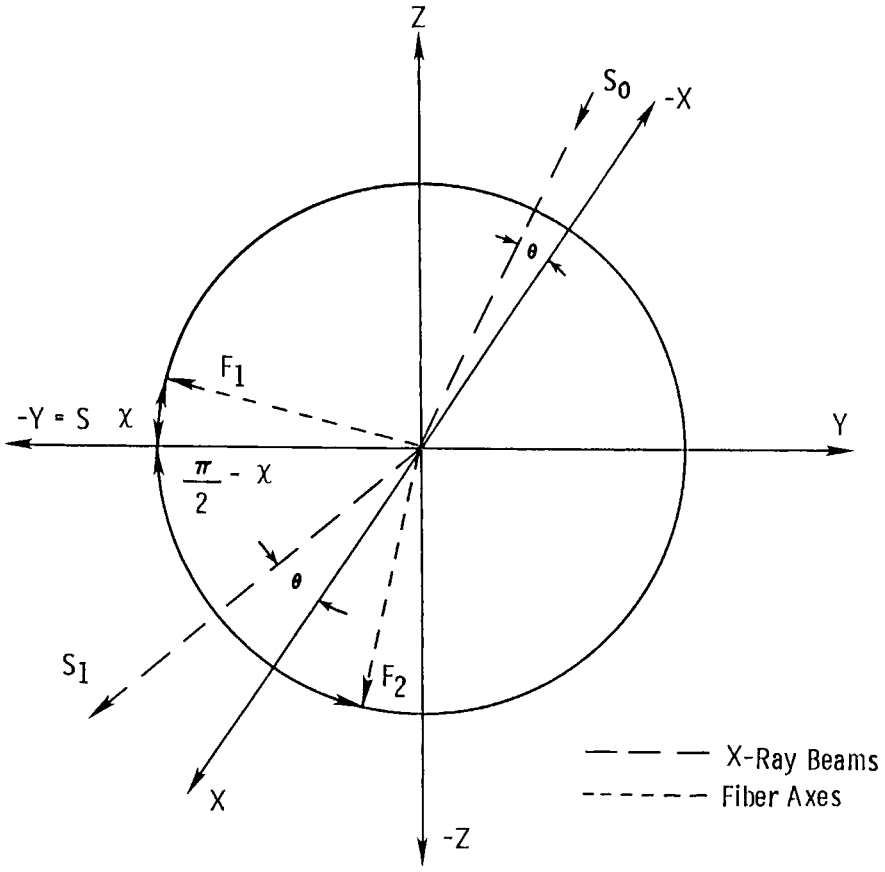

Figure 1 Diffractometer coordinate system showing symmetrical transmission mounting of a fabric specimen. **XYZ** are Cartesian coordinates. **X**, **Y**, $-\mathbf{X}$, $-\mathbf{Y} = \mathbf{S}$, $\mathbf{S}_0$, and $\mathbf{S}_1$ are all coplanar; **Y**, **Z**, $-\mathbf{Y} = \mathbf{S}$, $-\mathbf{Z}$, $\mathbf{F}_1$, and $\mathbf{F}_2$ are also all coplanar. (– – –), X-ray beams; (-----), fiber axes; (——), Cartesian coordinate axes.

point of impact. The diffraction data have been background corrected and then corrected by a Lorenz polarization correction.

DETERMINATION OF PHASE CONTENT

X_{amorph}, X_{mono}, and X_{orth} are defined as the mass fractions of amorphous, monoclinic, and orthorhombic phase material in the specimen, respectively, constrained to add up to unity. These quantities have been determined from the relative integrated areas A_{am}, A_{110}, A_{200}, and A_{001} of the amorphous, orthorhombic (110), orthorhombic (200), and monoclinic (001) peaks, respectively. The following equations were arrived at for the crystalline fractions:

$$X_{orth} = 1/(1 + R_a + R_m) \quad (1)$$

$$X_{mono} = R_m/(1 + R_a + R_m) \quad (2)$$

and

$$X_{amorph} = R_a/(1 + R_a + R_m) \quad (3)$$

In these equations, the ratio R_a is defined by

$$R_a \equiv X_{amorph}/X_{orth} = (A_{am}/2)/(A_{110} + A_{200}) \quad (4)$$

where the factor (1/2) is required to compensate for a peculiarity of the fabric randomization method and does not ordinarily appear for fiber or randomly oriented samples. This factor is discussed more fully in the Appendix.

The ratio R_m is defined by

$$R_m \equiv X_{mono}/X_{orth} = K_{fac}(A_{001}/A_{110}) \quad (5)$$

where K_{fac} is a combined factor for structure factor, multiplicity, and temperature and has the value 2.074. K_{fac} essentially corrects for the different intrinsic diffraction intensities of the monoclinic (001) and orthorhombic (110) planes; the remaining ratio R_m is attributable to the ratio of the mass fractions of the two phases.

The total crystallinity X_{cryst} is the sum of the orthorhombic and monoclinic crystalline fractions, given by

$$X_{cryst} \equiv X_{orth} + X_{mono}$$

APPLICATION OF THE CRYSTALLINITY DETERMINATION METHOD

The samples consisted of polyethylene fabric assembled into ballistic test panels of 35 layers of fabric. The engineering parameters of the test fabric panels are shown in Table I. The V_{50} velocity of the 0.22-caliber blunt projectile was in all instances in the vicinity of 1874 ft/s (571 m/s) for the penetration of the panels. V_{50} is the velocity where the probability of complete penetration is 50%. The intention was to study phenomena in the V_{50} critical region. Thus, the "incomplete penetration" data represents a projectile lacking enough velocity for complete penetration, while the "complete penetration" data represents a projectile having enough velocity for complete penetration. As previously mentioned, diffraction patterns were obtained for each sample at both the projectile damage zone and at an undamaged zone, the latter serving as a control.

Two typical diffraction patterns are shown in Figure 2. These patterns have been subjected to background and Lorenz polarization corrections. The vertical scale of the graph is X-ray counts, while the horizontal scale is the Bragg angle 2θ. The data acquisition time, 1 h 21 min 2 s, is an outcome of the computer algorithm used in data acquisition, resulting from specifying a maximum counting time of 60 s for any of the χ values, which range from 0–90° at 1° steps. Figure 2(a) is a typical pattern in which the monoclinic peak is present, while Figure 2(b) shows one in which that peak is absent.

The FORTRAN-program MCAMENU developed in this laboratory was used for data analysis. For each of the diffraction patterns, the areas of the crystalline peaks [orthorhombic (110) and (200) and monoclinic (001) peak if present] were evaluated by fitting the data within the region of the peak in an iterative fashion to a Gaussian curve combined with a linear baseline. The Lorentzian peak function was also tried, but these results were not used because the curve fit was poorer, as judged by a least-

Table I Engineering Parameters of Test Fabric Panels

Fiber grade	Spectra 1000™
Yarn denier	650
Weave	34 × 34 plain weave
Layers in test panel	35
Fabric areal density	
Per layer	206 g/cm² (6 oz/sq yd)
35-Layer panel	7210 g/cm² (210 oz/sq yd)

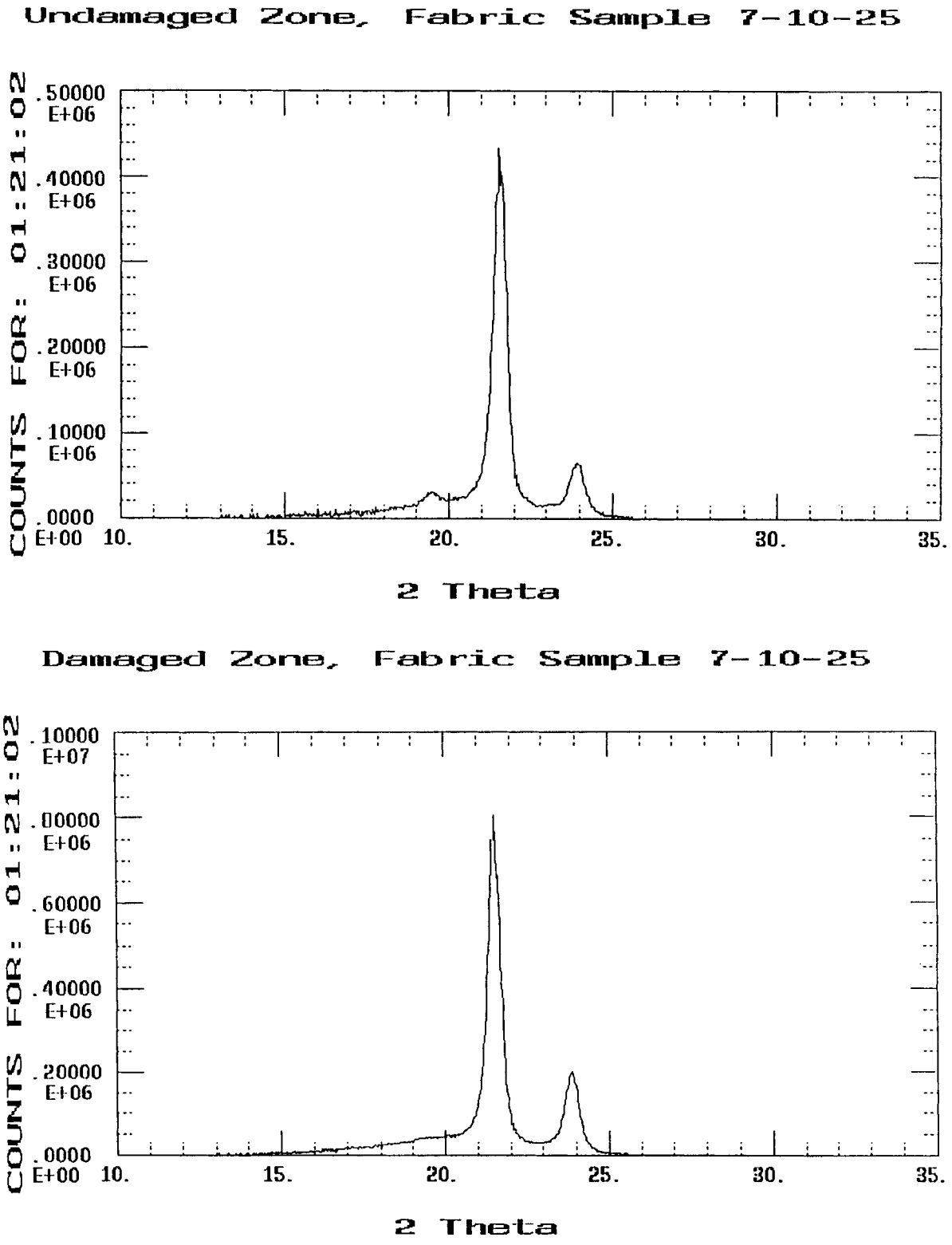

Figure 2 Two typical corrected diffraction patterns. (a) Pattern in which the monoclinic phase is present, (b) pattern in which the monoclinic phase is absent.

squares criterion, than the fit using a Gaussian curve. The results of each curve fit included the optimum peak position, intensity, full width at half maximum (FWHM), and area. Representative peak fit graphs, comparing experimental data with calculated curves, are shown in Figure 3. The parameters derived from the curve fit are listed in Table II.

The amorphous area is found by subtracting the three resolved crystalline areas from the total area of the experimental diffraction curve. The calculated mass fractions of the monoclinic, orthorhombic, and total crystalline phases for the patterns are shown in detail in Table III and summarized in Table IV. The sample crystallinity data, shown in Table III, is presented in terms of the values of the sample parameters in effect for each diffraction pattern: C or I for complete or incomplete penetration, the layer number, and D or U for a damaged or undamaged zone.

RESULTS

In the summary (Table IV), the mass fraction data are broken down into four classes for the four combinations of either complete or incomplete penetration and damaged or undamaged zones. Within each class, the average monoclinic and orthorhombic fractions are reported with their respective standard deviations. Table IV also includes the results of a replication experiment run to assess the reproducibility of the results. For this study, a single test specimen (7-5-5, incomplete penetration) was run at five different locations in its undamaged zone. The five different locations were used to assess the sampling effect, as well as experimental uncertainty.

The results for the replication experiment show a monoclinic fraction of 0.049 (SD 0.009) and an orthorhombic fraction of 0.741 (SD 0.018) for a total crystallinity of 0.790 (SD 0.013). It is of interest that the SD of the total crystallinity is lower than that of the orthorhombic fraction. Examination of the data in detail (Table III) reveals the explanation: For the five replicate determinations, low values of the monoclinic fraction correlate with high values of the orthorhombic fraction, and vice versa. In other words, as the fabric is sampled at different locations fluctuations in monoclinic fraction tend to correlate with fluctuations in orthorhombic fraction to hold the total crystallinity constant to within an SD of 0.013, even though the SD of the orthorhombic fraction is 0.018. This corroborates the two-step crystallization process hypothesis: First, a certain fraction (0.790 with an SD of 0.013) of orthorhombic crystals is formed; then, a small fraction (0.049 with an SD of 0.009) of these transform to the monoclinic form, without altering the total crystallinity, leaving a lower fraction (0.741 with an SD of 0.018) of orthorhombic crystals. Such a situation is analogous to the subtraction of background (in this case, the monoclinic fraction) from a signal (the total crystallinity) to yield a corrected signal (the orthorhombic fraction). The statistical rule is that the SD of the corrected signal (orthorhombic fraction) is the square root of the sum of the squares of the other two quantities; the result of this calculation gives an SD of the orthorhombic fraction of 0.016, quite comparable to the experimental value of 0.018.

Referring to Table IV, it is evident from the SD values that there are greater differences in the various crystallinity values for the damaged samples (classes C, D and I, D) than for the undamaged samples (classes C, U and I, U). The data were examined more closely to see if these differences were associated with the layer level of the fabric specimen in the panel. The relationship between layer level and the crystallinities (monoclinic, orthorhombic, and total) are shown graphically in Figures 4–6. From these graphs, it is evident that there is no systematic effect of layer position on the crystallinities. As is to be expected for a series of controls, the undamaged results show remarkable consistency in the crystallinity results with little change with respect to layer. The damaged results while showing large variations in all three crystallinities with layer level show no consistency in that pattern of variation.

In the context of variation in the damage zone crystallinities, it is important to consider (and disprove) the possibility that some of the supposed damage zone patterns were in fact measured from undamaged material due to inaccurate placement of the X-ray beam. This possibility is considered in the data shown in Table V. In this table are summarized from Table III only those X_{mono} and X_{orth} values for damage zones within 1 SD of the corresponding undamaged zone value as judged by the replication experiment of Table IV. The X_{cryst} values, being dependent upon the other two, are not considered. Only 4 damage zone X_{mono} or X_{orth} values of 32 such determinations lie within 1 SD. In contrast, for the 32 corresponding undamaged zone determinations 19, or 59%, of such values are within 1 SD of the replication experiment value. It is evident from the data in Table V that none of the damage zone patterns are, in fact, from undamaged material.

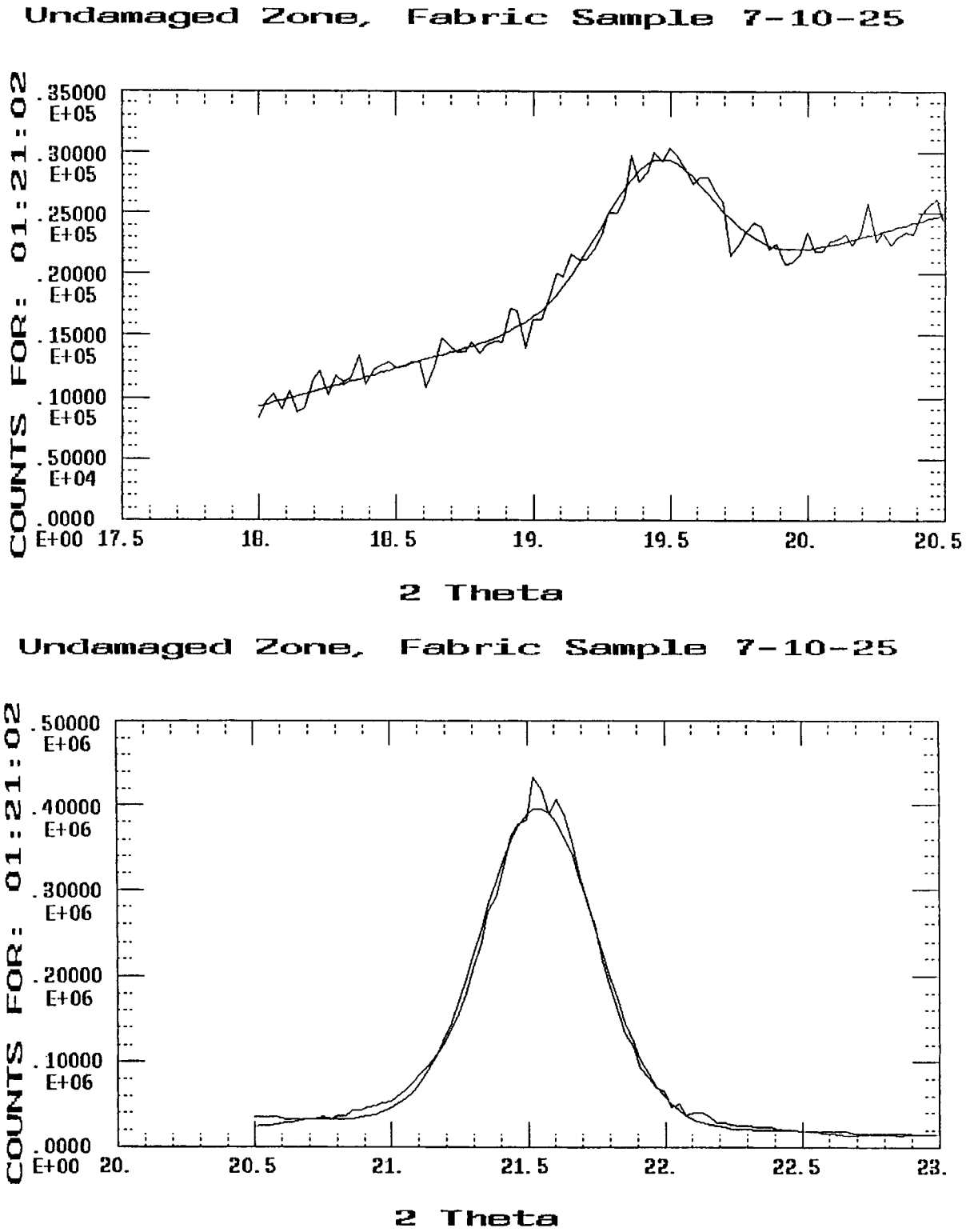

Figure 3 Curve fitting a Gaussian peak with linear baseline to experimental data. The smoother line is the calculated Gaussian peak. (a) monoclinic (001) peak, (b) orthorhombic (110) peak, (c) orthorhombic (200) peak.

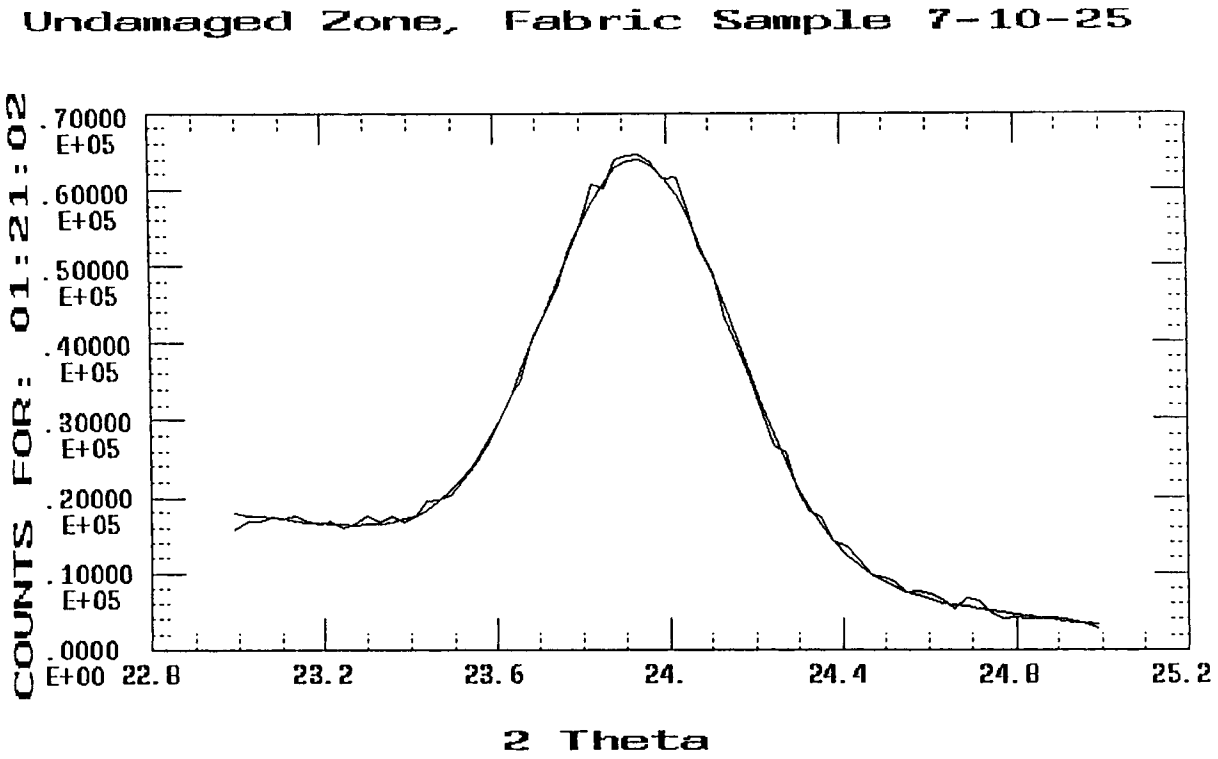

Figure 3 *(continued from the previous page)*

DISCUSSION

It should be noted at the outset that the results of all the patterns of undamaged material are in essential agreement at a monoclinic fraction of 0.04 and an orthorhombic fraction of 0.61, with no statistically significant difference between the complete, undamaged and incomplete, undamaged classes. All undamaged material patterns may be regarded as representative of virgin fabric unaffected by the ballistic impact.

In the damaged classes, two effects are apparent. First, the monoclinic fraction shows large variations from sample to sample, ranging from 0–0.132. Second, the orthorhombic fraction values are lower and show more variations than the undamaged patterns. To illustrate the first effect, in the complete, damaged class, five of the eight patterns showed no monoclinic fraction, while the remaining three showed monoclinic fractions of 0.047, 0.074, and 0.132. Illustrating the second effect, orthorhombic fractions in that same class ranged from 0.420–0.610 for the eight patterns.

Table II Guassian Curve-Fitting Parameters Derived from the Data of Figure 3

	Monoclinic (001)	Orthorhombic (110)	Orthorhombic (200)
Maximum intensity	11,079.0	369,856.0	52,952.0
Center position	19.448°	21.540°	23.936°
FWHM	0.478°	0.498°	0.509°
Gaussian area[a]	5637.0	196,056.0	28,715.0
Experimental area[b]	5797.0	198,220.0	28,815.0

[a] Calculated from the analytic Gauss function.

[b] Net area of the experimental curve after subtracting off the baseline area for the region examined.

Table III Monoclinic, Orthorhombic, and Total Crystalline Content of Polyethylene Fabric Samples from X-Ray Diffraction

Penetration	Layer	Damage State	X-Ray Mass Fractions		
			X_{mono}	X_{orth}	X_{cryst}
C	1	D	0.000	0.758	0.758
C	1	U	0.043	0.739	0.781
C	5	D	0.000	0.591	0.591
C	5	U	0.040	0.768	0.808
C	10	D	0.094	0.634	0.727
C	10	U	0.034	0.769	0.803
C	15	D	0.060	0.678	0.738
C	15	U	0.065	0.717	0.782
C	20	D	0.000	0.639	0.639
C	20	U	0.034	0.750	0.785
C	25	D	0.000	0.752	0.752
C	25	U	0.046	0.723	0.769
C	30	D	0.000	0.700	0.700
C	30	U	0.028	0.781	0.809
C	35	D	0.162	0.609	0.771
C	35	U	0.076	0.720	0.795
I	1	D	0.000	0.684	0.684
I	1	U	0.037	0.753	0.790
I	5	D	0.109	0.665	0.774
I	5	U	0.059	0.724	0.783
I	10	D	0.048	0.707	0.756
I	10	U	0.052	0.733	0.785
I	15	D	0.000	0.740	0.740
I	15	U	0.045	0.749	0.794
I	20	D	0.060	0.692	0.751
I	20	U	0.055	0.742	0.796
I	25	D	0.103	0.632	0.735
I	25	U	0.045	0.749	0.793
I	30	D	0.120	0.611	0.731
I	30	U	0.063	0.738	0.801
I	35	D	0.152	0.594	0.746
I	35	U	0.051	0.730	0.781

C, complete; I, incomplete, D, damaged; U, undamaged.

The changes in phase fractions brought about by ballistic impact are regarded as arising from very localized heating of the fabric due to the kinetic energy of the projectile. This heating can act in one of several ways. First, in the range of the well-known α transition of 60–100°C, associated with the onset of molecular chain motion in the crystallites, crystallite growth and annealing is possible. Second, when the normal melting point near 140°C of polyethylene is exceeded the polymer could melt and then recrystallize to some extent in the cooling process. However, there is a third possibility to consider, that of transformation to the hexagonal phase, reported by Clough[10] and Vaughan et al.[11] in the heating of crosslinked and stretched polyethylene. This phase is sometimes termed the "rotator" phase because the backbones of adjacent chains in the structure are rotated at random phase angles with respect to their neighboring chains. The stability of the hexagonal phase in preference to the melt phase requires an external constraint to hold the structure extended, but need not involve crosslinking: Murthy et al.[12] reported such a structure at 150–160°C in extended-chain polyethylene fibers held in tension by clamps. Upon cooling again, the hexagonal phase polyethylene would be expected to transform to orthorhombic crystallites unless mechanical working to promote the formation of monoclinic crystallites were present. The outcome would depend upon the thermal and mechanical history of each filament.

The data is interpreted as follows: In a few instances, where the monoclinic fraction well exceeds the undamaged value of 0.04, recrystallization has occurred, resulting in further growth of the monoclinic regions, perhaps at the expense of orthorhombic material, whose fraction generally drops with the ballistic event. Where the second or third process occurs, the monoclinic content is reduced or eliminated entirely.

Overall, the complete, damaged class show lower monoclinic fraction, and more instances of zero monoclinic fraction, than the incomplete, damaged class. This is taken to mean that when complete penetration occurs the filaments have been raised to a sufficiently high temperature to either melt the polymer or transform the crystallites to the hexagonal phase. Whether this is associated with the failure of the material cannot be determined from these data. Investigations of nylon fiber armor materials by Prosser[13,14] showed evidence of fiber frictional softening and indications that breaking of the yarns under tensile conditions is not necessarily the prime mode of failure under ballistic impact. In the present work, recrystallization is evident in the incomplete, damaged patterns in the fact that the average monoclinic fraction has increased to 0.059 over the undamaged value of 0.04. The increased scatter in the data for all the damaged patterns is indicative of differences in the ballistic impact event from one test to the next due to the unpredictable histories of individual filaments.

While the monoclinic phase is used here as a marker of thermomechanical history, the predomi-

Table IV Statistical Analysis: Monoclinic, Orthorhombic, and Total Crystalline Fraction Values

		Monoclinic Fraction		Orthorhombic Fraction		Total Crystallinity	
Class[a]	No.[b]	Average	SD	Average	SD	Average	SD
C, D	8	0.040	0.057	0.670	0.059	0.709	0.059
C, U	8	0.046	0.015	0.746	0.023	0.792	0.014
I, D	8	0.074	0.053	0.666	0.047	0.740	0.025
I, U	8	0.051	0.008	0.740	0.010	0.790	0.006
Replic.	5	0.049	0.009	0.741	0.018	0.790	0.013

[a] Abbreviations: C, D, complete, damaged; C, U, complete, undamaged; I, D, incomplete, damaged; I, U, incomplete undamaged; Replic., replication experiment.
[b] Number of determinations for each entry.

nant phase in all patterns is the well-known orthorhombic phase. Both the complete, damaged and incomplete, damaged classes show significant reduction in orthorhombic content compared to the undamaged fabric.

CONCLUSIONS

Both orthorhombic and monoclinic crystal content of high-tenacity ultrahigh-molecular-weight polyethylene fabrics have been successfully determined

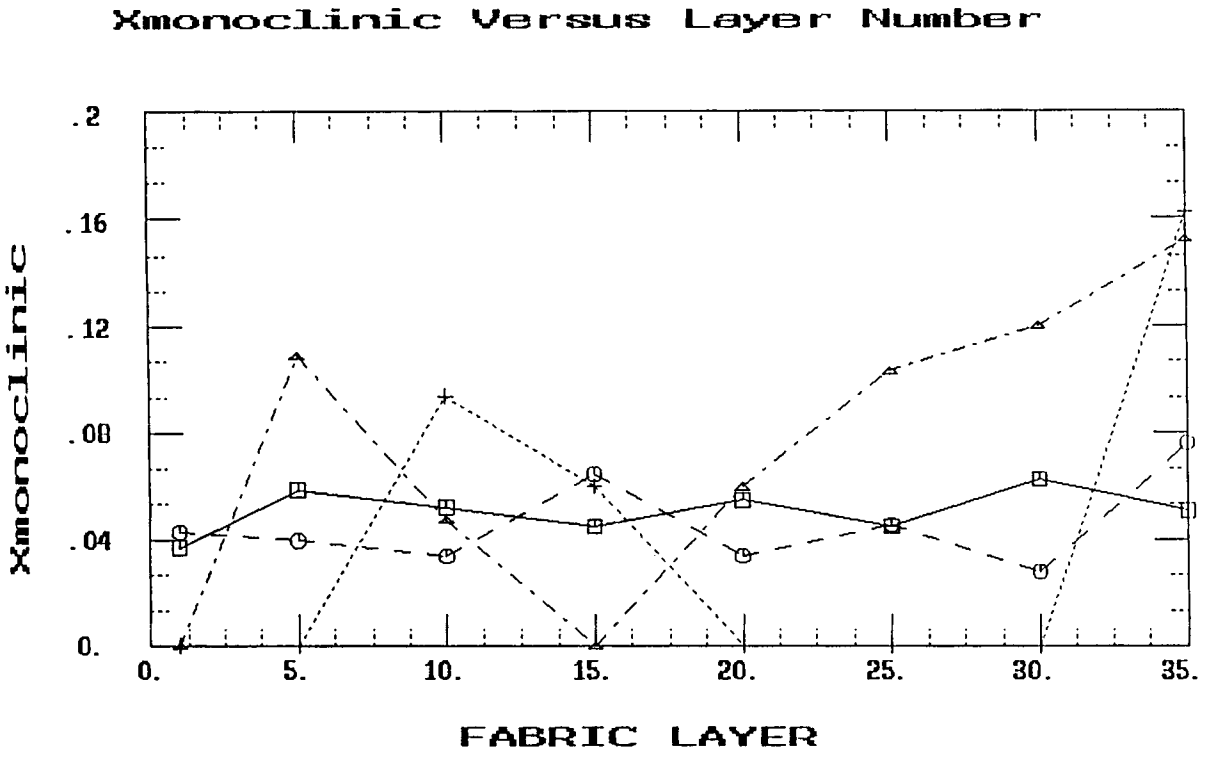

Figure 4 Plot of monoclinic crystalline fraction vs. fabric layer number. (——), undamaged area, incomplete penetration; (– – – –), undamaged area, complete penetration; (– – – –), damaged area, incomplete penetration; (– – – – –), damaged area, complete penetration.

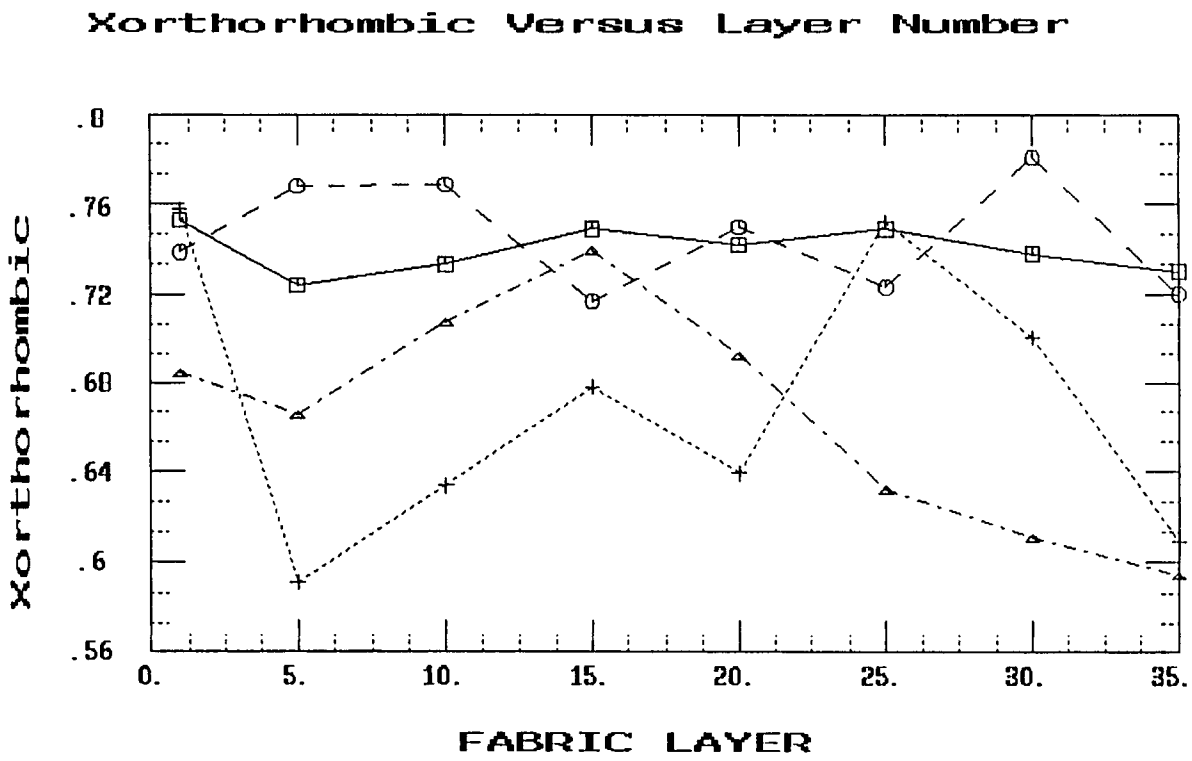

Figure 5 Plot of orthorhombic fraction vs. fabric layer number. Designation of lines vs. classes of Figure 4 applies.

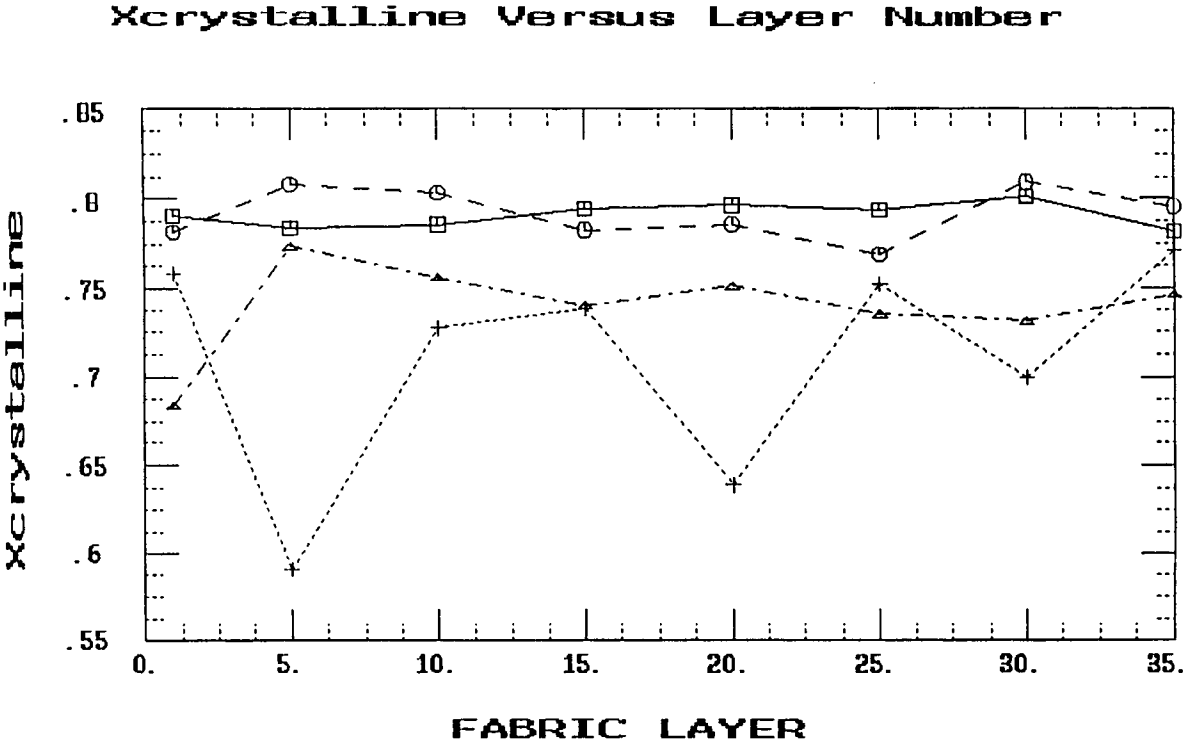

Figure 6 Plot of total crystalline fraction vs. fabric layer number. Designation of lines vs. classes of Figure 4 applies.

Table V Monoclinic and Orthorhombic Crystallinity Values for Damage Zones That are Near Replication Experiment Values

Penetration	Layer	Damage State	X-Ray Mass Fractions		
			X_{mono}	X_{orth}	X_{cryst}
C	1	D	0.000	0.758[a]	
C	25	D	0.000	0.752[a]	
I	10	D	0.048[a]	0.707	
I	15	D	0.000	0.740[a]	

C, complete; I, incomplete; D, damaged; U, undamaged.
[a] Value within 1 SD of the corresponding replication experiment value.

by a suitable X-ray diffraction method. The data for the metastable monoclinic phase is of particular interest as an indicator of thermal history effects in the ballistic event.

Crystallinity values for undamaged fabric are consistent within the precision of the determination and show an average orthorhombic fraction of 0.61 and an average monoclinic fraction of 0.04. Analogous determinations from damaged positions on the fabric show that ballistic impact can result in either an increase in monoclinic fraction, resulting from recrystallization near the normal polyethylene melting point, or eradication of monoclinic material, resulting from melting or transformation to the hexagonal phase. The latter predominates where ballistic penetration is complete.

Data from damaged fabric indicate that the major crystalline phase, the orthorhombic phase, is generally reduced in mass fraction by the ballistic impact event.

APPENDIX: X-RAY DIFFRACTION METHOD FOR CRYSTALLINITY DETERMINATION AS IMPLEMENTED FOR FABRIC SAMPLES

The method for averaging out the orientation effect in a fabric sample is a variation of the method used for fiber samples. For a fiber sample, we presume a single axis of cylindrical symmetry (the fiber axis) and denote χ as the angle between that axis and the diffraction vector **S** at a particular instrument setting. With this assumption, the experimental intensity may be written as $I(2\theta, \chi)$, a function of this fiber axis angle and the Bragg angle 2θ. The randomized intensity $I_{ave}(2\theta)$ *for a fiber sample* is properly found by the following weighted integration:

$$I_{ave}(2\theta) = (1/n) \int_0^{n\pi/2} I(2\theta, \chi) |\sin \chi| \, d\chi \quad \text{(A1)}$$

where n is the integral number of quandrants in χ over which data is averaged. The importance of the $\sin \chi$ weight factor has been shown by Desper and Stein[15]; its presence precludes the use of a simple spinning procedure that would weight all χ values equally. The method arrived at *for a fiber sample* to accomplish the necessary weighting is to vary the counting time used at each χ value in proportion to $|\sin \chi|$ so that each element of data in $I_{ave}(2\theta)$ is properly randomized.

For the present fabric sample problem, there are two sets (populations) of fibers, called set 1 and set 2, each set characterized by its own axis of symmetry, the two axes being at right angles. We shall assume that the fabric specimen is mounted on a diffractometer in the symmetrical transmission position, with the fabric plane bisecting the angle between the incident and diffracted beams, constraining the diffraction vector **S** to always lie in the fabric plane. The orientation angle χ shall be the variable rotational position of the fabric in the instrument as shown in Figure 1. The specimen is mounted in the diffractometer with the set 1 fiber axes parallel to the diffraction vector **S** at $\chi = 0$ and the set 2 fiber axes parallel to **S** at $\chi = \pi/2$. The experimental diffraction intensity at any $(2\theta, \chi)$ combination may be written as the sum of intensities from the two sets of fibers:

$$I_{exp}(2\theta, \chi) \equiv I_1(2\theta, \chi) + I_2(2\theta, \pi/2 - \chi) \quad \text{(A2)}$$

The terms $I_1(2\theta, \chi)$ and $I_2(2\theta, \pi/2 - \chi)$ are the intensity contributions from sets 1 and 2 of fibers, respectively. In this notation, the second parameter of the I_1 or the I_2 function is the angle between the fiber axis for that set and the instrument diffraction vector **S**.

Because the cylindrical symmetry axes for the two populations are at $\chi = 0$ and $\chi = \pi/2$, respectively, the properly randomized intensities for the two populations $\langle I_1 \rangle (2\theta)$ and $\langle I_2 \rangle (2\theta)$ are given by

$$\langle I_1 \rangle (2\theta) \equiv (1/n) \int_0^{n\pi/2} I_1(2\theta, \chi) |\sin \chi| \, d\chi \quad \text{(A3)}$$

and

$$\langle I_2\rangle(2\theta) \equiv (1/n)\int_0^{n\pi/2} I_2(2\theta, \pi/2 - \chi)|\cos\chi|d\chi \quad (A4)$$

The true randomized intensity, $\langle I\rangle(2\theta)$, may be written as the sum

$$\langle I\rangle(2\theta) \equiv \langle I_1\rangle(2\theta) + \langle I_2\rangle(2\theta) \quad (A5)$$

Let us consider the following weighted average $I_{exp}(2\theta)$ defined by

$$I_{exp}(2\theta) \equiv (1/n)\int_0^{n\pi/2} I(2\theta, \chi) \times (|\sin\chi| + |\cos\chi|)d\chi \quad (A6)$$

This intensity function may be measured experimentally by collecting data at each χ for a time proportional to the weighting function $(|\sin\chi| + |\cos\chi|)$. Difficulty arises from the fact that in the experimental $I_{exp}(2\theta)$ of eq. (A6) the intensities of the two populations are collectively weighted by the function $(|\sin\chi| + |\cos\chi|)$, while for the true randomization $\langle I\rangle(2\theta)$ the two populations are individually weighted by the functions $|\sin\chi|$ and $|\cos\chi|$.

In practice, a solution to this difficulty is not obtained in the general case but can be approximated for a special case as follows. Suppose each individual fiber intensity such as $I_1(2\theta, \chi)$ of eq. (A2) may be written as the sum of two contributions: an isotropic amorphous intensity $I_{1A}(2\theta)$ independent of χ and an equatorial crystalline phase intensity $I_{1C}(2\theta, \chi)$ that is a function of the orientation angle χ and, in particular, is strong only near the equatorial position, where the second parameter of either $I_1(2\theta, \chi)$ or $I_2(2\theta, \pi/2 - \chi)$ is $\pi/2$. Thus, we write

$$I_1(2\theta, \chi) = I_{1A}(2\theta) + I_{1C}(2\theta, \chi) \quad (A7)$$

and analogously for the set 2 fibers

$$I_2(2\theta, \pi/2 - \chi) = I_{2A}(2\theta) + I_{2C}(2\theta, \pi/2 - \chi) \quad (A8)$$

We may proceed to apply eqs. (A3) and (A4) to (A7) and (A8) to further evaluate the properly randomized intensity functions for the two fiber sets:

$$\langle I_1\rangle(2\theta) = I_{1A}(2\theta) + \langle I_{1C}\rangle(2\theta) \quad (A9)$$

and

$$\langle I_2\rangle(2\theta) = I_{2A}(2\theta) + \langle I_{2C}\rangle(2\theta) \quad (A10)$$

where we now define

$$\langle I_{1C}\rangle(2\theta) \equiv (1/n)\int_0^{n\pi/2} I_{1C}(2\theta, \chi)|\sin\chi|d\chi \quad (A11)$$

and

$$\langle I_{2C}\rangle(2\theta) \equiv (1/n)\int_0^{n\pi/2} I_{2C}(2\theta, \pi/2 - \chi)|\cos\chi|d\chi \quad (A12)$$

The quantities $\langle I_{1C}\rangle(2\theta)$ and $\langle I_{2C}\rangle(2\theta)$ defined in (A11) and (A12) are the properly randomized *crystalline* portions of the two fiber intensities. The true fabric randomized intensity $\langle I\rangle(2\theta)$ may now be written:

$$\langle I\rangle(2\theta) = I_{1A}(2\theta) + \langle I_{1C}\rangle(2\theta) + I_{2A}(2\theta) + \langle I_{2C}\rangle(2\theta) \quad (A13)$$

Substituting into (A2) and then into (A6)

$$\begin{aligned} I_{exp}(2\theta) = {} & [I_{1A}(2\theta) + I_{2A}(2\theta)] \\ & + (1/n)\int_0^{n\pi/2} I_{1C}(2\theta, \chi)|\sin\chi|d\chi \\ & + (1/n)\int_0^{n\pi/2} I_{1C}(2\theta, \chi)|\cos\chi|d\chi \\ & + (1/n)\int_0^{n\pi/2} I_{2C}(2\theta, \pi/2 - \chi)|\cos\chi|d\chi \\ & + (1/n)\int_0^{n\pi/2} I_{2C}(2\theta, \pi/2 - \chi)|\sin\chi|d\chi \quad (A14) \end{aligned}$$

Note that the equatorial position for strong crystalline diffraction occurs for the two sets of fibers where their respective angle parameters χ and $\pi/2 - \chi$ take on the value $\pi/2$, wehre each set of fibers is perpendicular to the diffractometer **S** vector. Provided the crystalline equatorial reflections are sufficiently sharp in their χ distributions, as we have assumed for this special case, the third and fifth terms on the right side of eq. (A14) will be negligible compared to the second and fourth terms. The experimental intensity is then approximated by

$$I_{exp}(2\theta) = 2[I_{1A}(2\theta) + I_{2A}(2\theta)] + (1/n)\int_0^{n\pi/2} I_{1C}(2\theta, \chi)|\sin\chi|d\chi + (1/n)\int_0^{n\pi/2} I_{2C}(2\theta, \pi/2 - \chi)|\cos\chi|d\chi \quad (A15)$$

Examining (A15), the second and third terms may be identified with $\langle I_1\rangle(2\theta)$ and $\langle I_2\rangle(2\theta)$ using (A11) and (A12), and eq. (A15) may be written

$$I_{exp}(2\theta) = 2[I_{1A}(2\theta) + I_{2A}(2\theta)] + \langle I_{1C}\rangle(2\theta) + \langle I_{2C}\rangle(2\theta) \quad (A16)$$

Comparing it with (A13), (A16) does not give a true randomization because of the factor 2 multiplying the amorphous contribution $[I_{1A}(2\theta) + I_{2A}(2\theta)]$. The problem we are faced with is that of separating this amorphous contribution from the remaining crystalline contribution $[\langle I_{1C}(2\theta) + \langle I_{2C}\rangle(2\theta)]$ from the experimental intensity curve $I_{exp}(2\theta)$. This problem has been dealt with over the years by a number of mathematical or graphical methods: see Matthew et al.,[16] Gopalan and Mandelkern,[17] and Hsieh et al.[18] The method used here, described in Hsieh et al.,[18] consists of fitting either Gauss or Cauchy (Lorentzian) line shape functions to the crystalline peaks and attributing the remaining intensity to amorphous scattering. Whatever method is used, we shall presume that there exists a mathematical operation that will separate $I_{exp}(2\theta)$ into two component curves $I_{exp,A}(2\theta)$ and $I_{exp,C}(2\theta)$, the amorphous and crystalline components, respectively. We may then identify

$$I_{exp,A}(2\theta) = 2[I_{1A}(2\theta) + I_{2A}(2\theta)] \quad (A17)$$

and

$$I_{exp,C}(2\theta) = \langle I_{1C}\rangle(2\theta) + \langle I_{2C}\rangle(2\theta) \quad (A18)$$

The problem is now solved in principle. We may identify the X-ray crystallinity X_C with the ratio of integrated randomized crystalline intensity to integrated randomized total intensity:

$$X_c = \frac{\int_0^{\pi/2} [\langle I_{1C}\rangle(2\theta) + \langle I_{2C}\rangle(2\theta)]d(2\theta)}{\int_0^{\pi/2} [I_{1A}(2\theta) + I_{2A}(2\theta) + \langle I_{1C}\rangle(2\theta) + \langle I_{2C}\rangle(2\theta)]d(2\theta)} \quad (A19)$$

which, in terms of experimental data, may be written

$$X_C = \frac{\int_0^{\pi/2} I_{exp,C}(2\theta)d(2\theta)}{\int_0^{\pi/2} \{[I_{exp,A}(2\theta)/2] + I_{exp,C}(2\theta)\}d(2\theta)} \quad (A20)$$

The notable feature of (A20) is the appearance of the factor of 2 dividing the experimental amorphous intensity $I_{exp,A}(2\theta)$. This artifact originates in the $(|\sin\chi| + |\cos\chi|)$ weighting function used in measuring the experimental intensities. When this weighting function is applied, each fiber set's amorphous intensity integrates as a constant with each of the trigonometric factors to give double its true randomized contribution, while each crystalline term interacts with only one of the trigonometric factors to give a single true randomized contribution. Thus, the amorphous contribution is overcounted by a factor of 2, which must be compensated for in the crystallinity calculation.

In the present data, with two crystalline phases present, the item of interest is R_a, defined as the ratio of amorphous to orthorhombic fractions. Taking into account the overcounting of the amorphous data, R_a will be given by

$$R_a = \frac{\int_0^{\pi/2} [I_{exp,A}(2\theta)/2]d(2\theta)}{\int_0^{\pi/2} [I_{exp,110}(2\theta) + I_{exp,200}(2\theta)]d(2\theta)} \quad (A21)$$

where the intensities in the denominator refer to the orthorhombic (110) and (200) reflections. Written in terms of integrated areas, (A21) becomes

$$R_a = (A_{am}/2)/(A_{110} + A_{200}) \quad (A22)$$

which was used in the present calculations.

REFERENCES

1. C. W. Bunn, *Trans. Faraday Soc.*, **35**, 482 (1939).
2. S. Kavesh and J. M. Schultz, *J. Polym. Sci. A-2*, **8**, 243 (1970).
3. W. R. Busing, *Macromolecules*, **23**, 4608 (1990).
4. W. P. Slichter, *J. Polym. Sci.*, **21**, 141 (1956).

5. K. Tanaka, T. Seto, and T. Hara, *J. Phys. Soc. Jpn.*, **17,** 873 (1962).
6. T. Seto, T. Hara, and K. Tanaka, *Jpn. J. Appl. Phys.*, **7,** 31 (1968).
7. J. H. Magill, S. S. Pollack, and D. P. Wyman, *J. Polym. Sci. A,* **3,** 3781 (1965).
8. J. G. Fatou, C. H. Baker, and L. Mandelkern, *Polymer,* **6,** 243 (1965).
9. W. T. Mead, C. R. Desper, and R. S. Porter, *J. Polym. Sci., Polym. Phys. Educ.,* **17,** 859 (1979).
10. S. B. Clough, *Polym. Lett.,* **8,** 519 (1970).
11. A. S. Vaughan, G. Ungar, D. C. Bassett, and A. Keller, *Polymer,* **26,** 726 (1985).
12. N. S. Murthy, S. T. Correale, and S. Kavesh, *Polym. Comm.,* **31,** 50 (1990).
13. R. A. Prosser, *Textile Res. J.,* **58,** 61 (1988).
14. R. A. Prosser, *Textile Res. J.,* **58,** 161 (1988).
15. C. R. Desper and R. S. Stein, *Polym. Lett.,* **5,** 893 (1967).
16. J. L. Mathews, H. S. Peiser, and R. B. Richards, *Acta Crystal.,* **2,** 85 (1949).
17. M. R. Gopalan and L. Mandelkern, *Polym. Lett.,* **5,** 925 (1967).
18. A. J. Hsieh, C. R. Desper, and N. S. Schneider, *Polymer,* **33,** 306 (1992).

Received February 4, 1992
Accepted April 29, 1992